IEEE Access
Multidisciplinary ⋮ Rapid Review ⋮ Open Access Journal

Received December 2, 2020, accepted December 17, 2020, date of publication December 24, 2020, date of current version January 8, 2021.

Digital Object Identifier 10.1109/ACCESS.2020.3047063

Model Analysis and Modified Control Method of Ship-Mounted Stewart Platforms for Wave Compensation

YUNFEI CAI[1], SHUTAO ZHENG[1], WEITIAN LIU[2], ZHIYONG QU[1], AND JUNWEI HAN[1]
[1]School of Mechanical and Electrical Engineering, Harbin Institute of Technology, Harbin 150080, China
[2]Aecc Aero Engine Control System Institute, Aero Engine Corporation of China, Wuxi 214000, China

Corresponding authors: Shutao Zheng (zhengst77@hit.edu.cn), Zhiyong Qu (hitqzy@163.com), and Junwei Han (hjw@hope.hit.edu.cn)

ABSTRACT Offshore installations e.g. marine transportation, oil platforms, etc. are strongly depended on sea conditions. To increase workable time of carrying out these operations, a Stewart platform is installed on a ship to serve as a motion compensation base and equipment on the base can have the same precision with those on the land-fixed base. Since movements of the Stewart platform are influenced by persistent ship motions, they present more complicated dynamical characteristics which make the control issue much more challenges. In the existing results, the established model does not consider the ship motion disturbances or is a linearized model, besides, the actuator velocity is also needed. In this paper, a modified control method is proposed for the ship-mounted Stewart platform. Specifically, the dynamics model considering ship motion disturbances is established and the influence of ship motions on the Stewart platform is analyzed. Through the model analysis, a modified motion controller is proposed with utilizing a multiple degrees of freedom velocity feedforward compensator. Finally, simulations are included to illustrate the effectiveness of the modified control method by contrast.

INDEX TERMS Motion compensation, ship-mounted Stewart platform, dynamics analysis, multiple degrees of freedom velocity feedforward.

I. INTRODUCTION

THERE is an increasing development for offshore industry such as oil platforms, wind turbines and offshore cranes, etc [1], [2]. For the above applications, loads and personnel have to be transferred from one ship to another, or between a ship and solid offshore structures. However, the above offshore operations are strongly depended on weather and sea conditions, which means low working efficiency and economic loss due to unworkable sea conditions [3]–[5]. e.g., for offshore crane operations, once the significant wave height reaches 1m to 1.5m on the Pierson-Moskowitz Sea Spectrum the crane operations have to be aborted due to undesirable pendulation of the cargo. Datas have been presented to show that typical crane ships in the North Sea have an available work time of no more than half a year. For the assembly and maintenance of wind turbines, it is required to hoist parts from a ship onto the fixed base of the wind turbine. Those parts can collide with the wind turbine and cause damage due to wave induced ship motions. To increase workable time of carrying out these operations, this paper proposes a solution Stewart platform to address the ship motions and wave induced ship motions can be compensated for. Then top platform can keep motionless in the inertial frame by controlling length of actuators and loads and personnel can be transferred more easily.

A ship at sea experiences some roll, pitch, surge, yaw, sway and heave motions in rough sea conditions [6], [7], which makes motion compensation difficult to carry out. Unlike traditional land-fixed Stewart platform systems, their bases are equipped on the ship deck, whose motions are influenced by sea waves and ocean currents, and they work in a non-inertial frame. This means that, to accurately carry out marine transportation, it is required to address the ship motions, which make the system dynamics more complex and stronger nonlinearity. Hence, traditional control methods for land-fixed mechanical systems are unapplicable to ship-mounted Stewart platforms and controller design becomes a more challenging problem.

The associate editor coordinating the review of this manuscript and approving it for publication was Zheng H. Zhu.

Over the last few decades, control problems for land-fixed mechanical systems have been extensively investigated, and many ambitious fruits have been reported in the literature. Fewer results have been reported for mechanical systems operated in the non-inertia frame, due to their complicated dynamical characteristics, strong nonlinearity and unexpected disturbances. However, we can still find some results reported for ship-mounted mechanical systems (e.g., offshore cranes). Kuchler *et al.* [8] put forward an active control approach for single degree of freedom motion compensation system by properly predicting the ship movements. Many control methods were proposed for the offshore crane systems to address problems of parametric uncertainties and persistent ship-induced perturbations, and asymptotic convergence results are obtained [3]–[5], [9], [10]. Compared with vertical motion compensation systems and offshore crane systems, the ship-mounted Stewart platforms have more complicated dynamics and more parametric uncertainties which make the controller design a more difficult task. Salzmann [11] proposed the idea of using the Stewart platform as a motion compensation system and safety philosophy and two methods of dimension synthesis were investigated. Madsen and Kristensen [12] investigated kinematic optimization and design for Stewart platforms with different configurations with respect to the global condition index and global manipulability index. Chang *et al.* [13] investigated compensation space based on the kinematic model. Wei *et al.* [14] investigated a method of solving inverse kinematics based on fuzzy algorithm for a hybrid boarding system which is a combination of a ship-mounted Stewart platform and a 3-DOF tandem manipulator, the problem of kinematical redundant is addressed. Zhao *et al.* [15] investigated a 6-degree-of-freedom foldable parallel mechanism for the ship-based stabilized platform, and stiffness and singularity analysis are carried out. Campos *et al.* [16] investigated helicopter floating helideck based on Stewart-Gough platform used as an active helideck upon landing on and taking off from ships or from offshore, a simple kinematics control method was used. Lie [17] investigated inverse dynamics control for the Ampelmann system to reduce undesired residual motions of top platform. According to the literature review above [11]–[17], dimension synthesis of the ship-mounted Stewart platform has been investigated deeply. But for the control problem of ship-mounted Stewart platform, the dynamic models in the existing results do not consider the influence of the ship motion disturbances or are a linearized model. In practice, ship motions resulting from sea waves will unavoidably degrade the control performance or lead to closed-loop instability. Moreover, existing results need the actuator velocity for the controller design which cannot obtain directly. Hence, high-performance control for ship-mounted Stewart platforms is still an open problem.

In this paper, we investigate stabilization scheme for a ship-mounted Stewart platform with the unmatched sea wave disturbances. Specifically, a nonlinear dynamics model is first set up for the Stewart platform with the influence of ship motions considered. Through model analysis, a multiple degrees of freedom velocity feedforward compensator is proposed. Then, a modified control method based on the velocity feedforward is developed. Finally, comparative simulation results are provided to illustrate the effectiveness of the modified control method.

Specifically, the contributions and novelties of the brief reside in the following aspects:

(1) Different from the aforementioned models in [17], the proposed dynamics model for ship-mounted Stewart platforms fully consider the influence of ship motions on Stewart platform.

(2) The influence of ship motions on the Stewart platform is **first** analyzed.

(3) Unlike the existing idea in [16], [17], a multiple degrees of freedom velocity feedforward compensator is **first** proposed.

(4) The modified control method does not need a large amount of sensor information i.e. velocity and acceleration of actuators in [17], which facilitates engineering application.

The reminder of this paper is organized as follows: In Section II, the complete dynamics model of the ship-mounted Stewart platform is set up. Section III, model analysis and controller design are carried out. Section IV provides some simulation results to illustrate model analysis results and performance of the ship-mounted Stewart platform controller, and Section V gives the conclusions of this paper.

Notations. Throughout the paper, S_α and C_α are utilized to denote functions $\sin\alpha$ and $\cos\alpha$, respectively; $\boldsymbol{S}(\boldsymbol{v})$ denotes a skew symmetric matrix of vector $\boldsymbol{v}$, diag $(\boldsymbol{k})$ is a corresponding diagonal matrix of a vector $\boldsymbol{k}$.

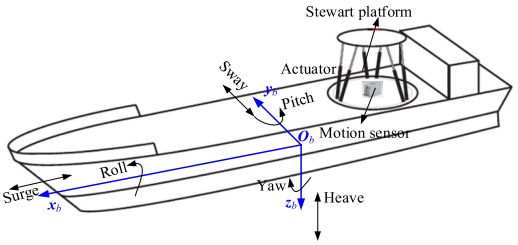

FIGURE 1. Ship-mounted Stewart platform system.

II. DYNAMICS MODEL OF THE SHIP-MOUNTED STEWART PLATFORM

A. KINEMATICS ANALYSIS

As shown in Fig.1, a Stewart platform is mounted on a ship's deck to keep top platform motionless relative to the inertial reference frame by changing length of actuators. The ship motions (roll, pitch, surge, yaw, sway and heave) can be measured with a motion sensor unit (e.g, Octans III), which has three accelerometers for detecting surge, sway, and heave and three rotation rate sensors for measuring roll, pitch, and yaw. The acceleration signals are double integrated to obtain

the positions of a ship as feedback signal and the rotation rate signals are integrated once to obtain the rotations. After continuously measuring the ship's position and orientation with respect to the inertial reference frame, then control the lengths of actuators to counteract the ship's movements.

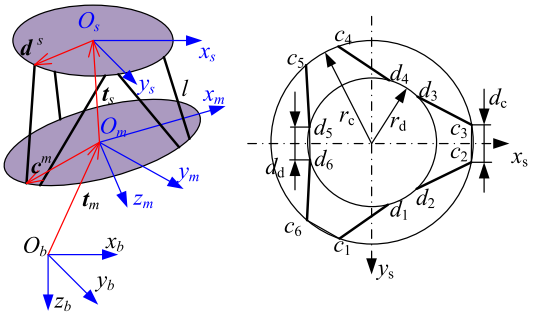

FIGURE 2. Coordinate system and geometric parameters.

In order to reflect the effect of ship motion on the Stewart platform, three coordinate frames including the inertial reference frame $\{O_b\}$, the ship coordinate frame $\{O_m\}$ and the platform coordinate frame $\{O_s\}$ are defined in Fig.2. In the frame $\{O_m\}$, the origin of the ship coordinate frame is the center of a motion sensor unit and the x_m-axis points to the forehead, which is also the forward moving direction of the ship, whereas the z_m-axis is perpendicular to the deck. Furthermore, to describe the ship position and orientation with respect to $\{O_b\}$, a generalized displacement is defined as $\boldsymbol{q}_b = (\psi_b, \theta_b, \varphi_b, x_b, y_b, z_b)^{\mathrm{T}}$. The orientation between the two frames of $\{O_m\}$ and $\{O_b\}$ is described by Euler angles $(\psi_b, \theta_b, \varphi_b)$. Additionally, for the translation of the ship relative to $\{O_b\}$, we utilize a vector $\boldsymbol{t}_m$ to denote the displacement $(x_b, y_b, z_b)^{\mathrm{T}}$. Therefore, the Euler transformation matrix between the inertial reference frame and the ship coordinate frame $\boldsymbol{R}_{bm}$ can be given by (1), as shown at the bottom of the page.

Similarly, the origin of the platform coordinate frame $\{O_s\}$ is the center of the upper gimbal points, with its axis parallel with the corresponding axis in the frame $\{O_m\}$. A generalized displacement is defined by $\boldsymbol{q}_s = (\psi_s, \theta_s, \varphi_s, x_s, y_s, z_s)^{\mathrm{T}}$ to describe position and orientation of the top platform with respect to $\{O_m\}$. The orientation between the two frames of $\{O_s\}$ and $\{O_m\}$ is described by Euler angles $(\psi_s, \theta_s, \varphi_s)$. For the translation of the top platform relative to $\{O_m\}$, we utilize a vector $\boldsymbol{t}_s$ to denote the displacement $(x_s, y_s, z_s)^{\mathrm{T}}$. Similarly, the Euler transformation matrix between the platform coordinate system and the ship coordinate system $\boldsymbol{R}_{ms}$ can also be given out, (2), as shown at the bottom of the page.

The inertial reference frame $\{O_b\}$ is fixed on the ground, with the x_b-axis parallel with the x_m-axis and the z_b-axis parallel with the z_m-axis.

Finally, a generalized displacement is defined as $\boldsymbol{q} = (\psi, \theta, \varphi, x, y, z)^{\mathrm{T}}$ to describe the position and orientation top platform with respect to the inertial reference frame, and the Euler transformation matrix and position vector are $\boldsymbol{R}$ and $\boldsymbol{t}$, respectively. Due to the six identical limbs, the following analysis focuses on the moving platform and one limb, and the symbol 'i' is omitted in the dynamics model process. However, other limbs are considered later in the complete dynamics model. Considering practical applications, motion compensation system cannot completely compensate the motion of the ship, top platform will move more or less. Here the purpose of kinematics analysis is to determine positions and velocities of each components given generalized displacements $\boldsymbol{q}_s$, $\boldsymbol{q}_b$. In order to obtain a simpler form of expression, all vectors are expressed in the ship coordinate system.

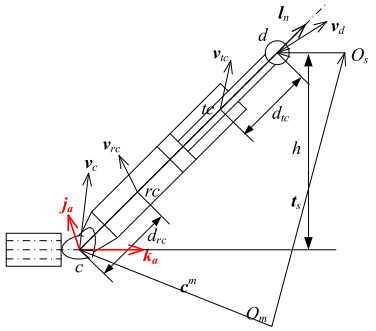

FIGURE 3. One limb of the ship-mounted Stewart Platform.

From Fig. 3, position of gimbal joint c_i and d_i $(i = 1, 2 \ldots 6)$ expressed in the ship coordinate system can be given by

$$\boldsymbol{c} = \boldsymbol{R}_{bm}^{T}\boldsymbol{t}_m + \boldsymbol{c}^m \tag{3}$$

$$\boldsymbol{d} = \boldsymbol{R}_{bm}^{T}\boldsymbol{t}_m + \boldsymbol{t}_s + R_{ms}\boldsymbol{d}^s \tag{4}$$

where $\boldsymbol{c}^m$ is position of gimbal joint c_i in the ship coordinate system and $\boldsymbol{d}^s$ is position of gimbal joint d_i in the platform coordinate frame. Therefore, the actuator length can be obtained

$$l = \left\| \boldsymbol{t}_s + \boldsymbol{R}_{ms}\boldsymbol{d}^s - \boldsymbol{c}^m \right\| \tag{5}$$

$$\boldsymbol{R}_{bm} = \begin{bmatrix} c\psi_b \cdot c\theta_b & c\psi_b \cdot s\theta_b \cdot s\varphi_b - s\psi_b \cdot c\varphi_b & s\psi_b \cdot s\varphi_b + c\psi_b \cdot s\theta_b \cdot c\varphi_b \\ s\psi_b \cdot c\theta_b & c\psi_b \cdot c\varphi_b + s\psi_b \cdot s\theta_b \cdot s\varphi_b & s\psi_b \cdot s\theta_b \cdot c\varphi_b - c\psi_b \cdot s\varphi_b \\ -s\theta_b & c\theta_b \cdot s\varphi_b & c\theta_b \cdot c\varphi_b \end{bmatrix} \tag{1}$$

$$\boldsymbol{R}_{ms} = \begin{bmatrix} c\psi_s \cdot c\theta_s & c\psi_s \cdot s\theta_s \cdot s\varphi_s - s\psi_s \cdot c\varphi_s & s\psi_s \cdot s\varphi_s + c\psi_s \cdot s\theta_s \cdot c\varphi_s \\ s\psi_s \cdot c\theta_s & c\psi_s \cdot c\varphi_s + s\psi_s \cdot s\theta_s \cdot s\varphi_s & s\psi_s \cdot s\theta_s \cdot c\varphi_s - c\psi_s \cdot s\varphi_s \\ -s\theta_s & c\theta_s \cdot s\varphi_s & c\theta_s \cdot c\varphi_s \end{bmatrix} \tag{2}$$

Angular velocity of top platform $\boldsymbol{\omega}_s$ can be written as

$$\boldsymbol{\omega}_s = \boldsymbol{R}_{bm}^T \boldsymbol{\omega}_m + \boldsymbol{\omega}_{sm} \tag{6}$$

where $\boldsymbol{\omega}_m$ denotes the angular velocity of base platform expressed in the inertial reference frame; $\boldsymbol{\omega}_{sm}$ denotes the angular velocity of top platform relative to base platform expressed in the ship coordinate frame. Furthermore, (6) can be written as

$$\boldsymbol{\omega_s} = \left[\boldsymbol{J}_{\omega sm}, \boldsymbol{R}_{bm}^T \boldsymbol{J}_{\omega m}\right] \dot{\boldsymbol{q}} = \boldsymbol{J}_{\omega s} \dot{\boldsymbol{q}} \tag{7}$$

With

$$\begin{aligned} \boldsymbol{J}_{\omega m} &= \begin{bmatrix} 0 & -\sin\psi_b & \cos\psi_b \cos\theta_b & 0 & 0 & 0 \\ 0 & \cos\psi_b & \sin\psi_b \cos\theta_b & 0 & 0 & 0 \\ 1 & 0 & -\sin\theta_b & 0 & 0 & 0 \end{bmatrix} \\ \boldsymbol{J}_{\omega sm} &= \begin{bmatrix} 0 & -\sin\psi_s & \cos\psi_s \cos\theta_s & 0 & 0 & 0 \\ 0 & \cos\psi_s & \sin\psi_s \cos\theta_s & 0 & 0 & 0 \\ 1 & 0 & -\sin\theta_s & 0 & 0 & 0 \end{bmatrix} \end{aligned} \tag{8}$$

where $\boldsymbol{J}_{\omega s}$ denotes the Jacobian matrix of the angular velocity of top platform, and $\boldsymbol{q} = \left(\boldsymbol{q}_s^T, \boldsymbol{q}_b^T\right)^T$.

It is not hard that in the ship coordinate frame, velocity of gimbal point c_i can be written as

$$\begin{aligned} \boldsymbol{v}_c &= \left(\boldsymbol{R}_{bm}^T \boldsymbol{J}_{tm} - \boldsymbol{S}\left(\boldsymbol{c}^m\right) \boldsymbol{R}_{bm}^T \boldsymbol{J}_{\omega m}\right) \dot{\boldsymbol{q}}_b = \boldsymbol{J}_{cb} \dot{\boldsymbol{q}}_b \\ &= \left[0_{3\times 6}, \boldsymbol{J}_{cb}\right] \dot{\boldsymbol{q}} \end{aligned} \tag{9}$$

Similarly, velocity of gimbal point d_i can be given by (10), as shown at the bottom of the page, where $\boldsymbol{J}_{tm} = \boldsymbol{J}_{ts} = [\boldsymbol{0}_{3\times 3}, \boldsymbol{I}_{3\times 3}]$, and $\boldsymbol{I}$ denotes a 3×3 unit matrix.

On the other hand, the velocity of gimbal point d_i can also be written as

$$\boldsymbol{v}_d = \boldsymbol{v}_c + \dot{l}\boldsymbol{l}_n + \boldsymbol{\omega}_a \times l\boldsymbol{l}_n \tag{11}$$

where $\boldsymbol{l}_n$ is a unit vector in the actuator direction, $\boldsymbol{\omega}_a$ is the angular velocity of the actuator relative to the inertial reference frame. Multiplying both sides of (12) with $\boldsymbol{l}_n$, the actuator velocity can be obtained

$$\dot{l} = = \boldsymbol{l}_n^T \left(\boldsymbol{J}_{ts} - \boldsymbol{S}\left(\boldsymbol{R}_{ms}\boldsymbol{d}^s\right) \boldsymbol{J}_{\omega sm}\right) \dot{\boldsymbol{q}}_s = \boldsymbol{J}\left(i, :\right) \dot{\boldsymbol{q}}_s \tag{12}$$

where $\boldsymbol{J}(i, :)$ denotes the i^{th} row of matrix $\boldsymbol{J}$. The matrix $\boldsymbol{J}$ is defined as the system Jacobian matrix. Similar to (11), the centroid velocity of top platform can be written as (13), shown at the bottom of the page, where $\boldsymbol{\rho}^s$ denotes the position vector of the centroid of the top platform in the platform coordinate frame.

In order to obtain angular velocity of the actuator relative to base platform, we decompose the angular velocity into a component perpendicular to the actuator direction and the other component along the actuator direction. Therefore, angular velocity of the actuator relative to base platform $\boldsymbol{\omega}_{ar}$ can be written as

$$\boldsymbol{\omega}_{ar} = \boldsymbol{\omega}_{arv} + \omega_{arn} \boldsymbol{l}_n \tag{14}$$

where ω_{sav} and ω_{san} denote the component perpendicular to the actuator direction and the value of the component along the actuator direction, respectively.

Obviously, the following expressions can be obtained

$$\boldsymbol{\omega}_{arv} = \frac{\boldsymbol{S}\left(\boldsymbol{l}_n\right)\left(\boldsymbol{J}_{ts} - \boldsymbol{S}\left(\boldsymbol{R}_{ms}\boldsymbol{d}^s\right)\boldsymbol{J}_{\omega sm}\right)}{l} \dot{\boldsymbol{q}}_s = \boldsymbol{J}_{arv} \dot{\boldsymbol{q}}_s \tag{15}$$

On the other hand, ω_{ar} can also be written as [18]

$$\boldsymbol{\omega}_{ar} = \omega_k \boldsymbol{k}_a + \omega_j \boldsymbol{j}_a \tag{16}$$

where $\boldsymbol{k}_a$ and $\boldsymbol{j}_a$ denote the direction vectors of two revolute joints of a universal joint, and $\boldsymbol{j}_a \perp \boldsymbol{l}_n$. Considering (14)-(16), ω_{san} can be obtained

$$\boldsymbol{\omega}_{san} = \frac{\boldsymbol{h}_a^T\left(-\boldsymbol{J}_{arv}\right)}{\boldsymbol{l}_n^T \boldsymbol{h}_a} \dot{\boldsymbol{q}}_s \tag{17}$$

where $\boldsymbol{h}_a = \boldsymbol{k}_a \times \boldsymbol{j}_a$. Therefore, Jacobian matrix of angular velocity of the actuator relative to base platform can be resolved as

$$\boldsymbol{J}_{\omega ar} = \boldsymbol{J}_{\omega arv} + \frac{\boldsymbol{l}_n \boldsymbol{h}_a^T\left(-\boldsymbol{J}_{arv}\right)}{\boldsymbol{l}_n^T \boldsymbol{h}_a} = \boldsymbol{J}_{\omega arv} + \boldsymbol{J}_{\omega arn} \tag{18}$$

Furthermore, angular velocity of the actuator relative to the inertial reference frame can be obtained

$$\boldsymbol{\omega}_a = \boldsymbol{\omega}_{ar} + \boldsymbol{\omega}_m = \left[\boldsymbol{J}_{\omega ar}, \boldsymbol{R}_{bm}^T \boldsymbol{J}_{\omega m}\right] \dot{\boldsymbol{q}} = \boldsymbol{J}_{\omega a} \dot{\boldsymbol{q}} \tag{19}$$

Ultimately, the centroid velocity of piston rod and cylinder tube can be obtained

$$\boldsymbol{v}_{rc} = \left(\left[0_{3\times 6}, \boldsymbol{J}_{cb}\right] - d_{rc} \boldsymbol{S}\left(\boldsymbol{l}_n\right) \boldsymbol{J}_{\omega a}\right) \dot{\boldsymbol{q}} = \boldsymbol{J}_{rc} \dot{\boldsymbol{q}} \tag{20}$$

$$\boldsymbol{v}_{tc} = \left(\boldsymbol{J}_d + d_{tc} \boldsymbol{S}\left(\boldsymbol{l}_n\right) \boldsymbol{J}_{\omega a}\right) \dot{\boldsymbol{q}} = \boldsymbol{J}_{tc} \dot{\boldsymbol{q}} \tag{21}$$

where d_{rc} denotes the distance between centroid of cylinder rod and point c_i; d_{tc} denotes the distance between centroid of cylinder tube and point d_i.

Here we still need to describe the velocity vectors in the inertial reference frame to obtain dynamics equation based on Kane method, and they are written as

$$\boldsymbol{\omega}_s = \left[\boldsymbol{R}_{bm} \boldsymbol{J}_{\omega sm}, \boldsymbol{J}_{\omega m}\right] \dot{\boldsymbol{q}} = \boldsymbol{J}_{\omega s} \dot{\boldsymbol{q}} \tag{22}$$

$$\boldsymbol{v}_p = \boldsymbol{R}_{bm} \boldsymbol{J}_p \dot{\boldsymbol{q}} = \boldsymbol{J}_p \dot{\boldsymbol{q}} \tag{23}$$

$$\boldsymbol{\omega}_a = \left[\boldsymbol{R}_{bm} \boldsymbol{J}_{\omega ar}, \boldsymbol{J}_{\omega m}\right] \dot{\boldsymbol{q}} = \boldsymbol{J}_{\omega a} \dot{\boldsymbol{q}} \tag{24}$$

$$\boldsymbol{v}_{rc} = \boldsymbol{R}_{bm} \boldsymbol{J}_{rc} \dot{\boldsymbol{q}} = \boldsymbol{J}_{rc} \dot{\boldsymbol{q}} \tag{25}$$

$$\boldsymbol{v}_{tc} = \boldsymbol{R}_{bm} \boldsymbol{J}_{tc} \dot{\boldsymbol{q}} = \boldsymbol{J}_{tc} \dot{\boldsymbol{q}} \tag{26}$$

$$\boldsymbol{v}_d = \left[\boldsymbol{J}_{ts} - \boldsymbol{S}\left(\boldsymbol{R}_{ms}\boldsymbol{d}^s\right)\boldsymbol{J}_{\omega sm}, \boldsymbol{R}_{bm}^T \boldsymbol{J}_{tm} - \boldsymbol{S}\left(\boldsymbol{t}_s\right)\boldsymbol{R}_{bm}^T \boldsymbol{J}_{\omega m} - \boldsymbol{S}\left(\boldsymbol{R}_{ms}\boldsymbol{d}^s\right)\boldsymbol{R}_{bm}^T \boldsymbol{J}_{\omega m}\right] = \boldsymbol{J}_d \dot{\boldsymbol{q}} \tag{10}$$

$$\boldsymbol{v}_p = \left[\boldsymbol{J}_{ts} - \boldsymbol{S}\left(\boldsymbol{R}_{ms}\boldsymbol{\rho}^s\right)\boldsymbol{J}_{\omega sm}, \boldsymbol{R}_{bm}^T \boldsymbol{J}_{tm} - \boldsymbol{S}\left(\boldsymbol{t}_s\right)\boldsymbol{R}_{bm}^T \boldsymbol{J}_{\omega m} - \boldsymbol{S}\left(\boldsymbol{R}_{ms}\boldsymbol{\rho}^s\right)\boldsymbol{R}_{bm}^T \boldsymbol{J}_{\omega m}\right] = \boldsymbol{J}_p \dot{\boldsymbol{q}} \tag{13}$$

In order to carry out acceleration analysis, the time derivative of two unit vectors need to be given out

$$\dot{\boldsymbol{l}}_n = \boldsymbol{S}(\boldsymbol{\omega}_{ar})\boldsymbol{l}_n \tag{27}$$

$$\dot{\boldsymbol{h}}_a = \boldsymbol{k}_a \times (\boldsymbol{\omega}_{ar} \times \boldsymbol{j}_a) \tag{28}$$

Then, the time derivative of Jacobian matrix $\boldsymbol{J}_p$ can be obtained in (29), as shown at the bottom of the page, with, (30) and (31), as shown at the bottom of the page.

The centroid acceleration of top platform can be calculated with

$$\dot{\boldsymbol{v}}_p = \boldsymbol{J}_p\ddot{\boldsymbol{q}} + \dot{\boldsymbol{J}}_p\dot{\boldsymbol{q}} \tag{32}$$

The actuator acceleration can be calculated by differentiating (13)

$$\ddot{\boldsymbol{l}} = \boldsymbol{J}\ddot{\boldsymbol{q}}_s + \dot{J}\dot{\boldsymbol{q}}_s \tag{33}$$

using, (34), as shown at the bottom of the page.

In order to calculate centroid acceleration of the piston rod and cylinder tube, differentiating (17)-(19) yields the following equations, (35)–(39), as shown at the bottom of the page.

Centroid acceleration of piston rod and cylinder tube can be given by

$$\dot{\boldsymbol{v}}_{rc} = \dot{\boldsymbol{J}}_{rc}\dot{\boldsymbol{q}} + \boldsymbol{J}_{rc}\ddot{\boldsymbol{q}} \tag{40}$$

$$\dot{\boldsymbol{v}}_{tc} = \dot{\boldsymbol{J}}_{tc}\dot{\boldsymbol{q}} + \boldsymbol{J}_{tc}\ddot{\boldsymbol{q}} \tag{41}$$

B. DYNAMICS ANALYSIS

Through the previous kinematics analysis, it can be seen that velocity Jacobian matrices consist of two parts: one for $\dot{\boldsymbol{q}}_s$ and the other for $\dot{\boldsymbol{q}}_b$; therefore they have a form of $[\boldsymbol{J}_s, \boldsymbol{J}_b]$, e.g. $\boldsymbol{J_p} = [\boldsymbol{J_{ps}}, \boldsymbol{J_{pb}}]$ and both $\boldsymbol{J_{ps}}$ and $\boldsymbol{J_{pb}}$ are 3×6 matrices.

In order to reduce the computational complexity and facilitate programming, we establish dynamics model by applying Kane method. Here the inertia force, the inertia moment and the gravity as well as the actuation force are projected into the task space through the Jacobian matrices as the generalized inertia force and the generalized driving force. Then, the dynamics equation is established based on the D'Alembert Theory.

The generalized inertia force of top platform can be given by, (42), as shown at the bottom of the next page, where m_p denotes the mass of top platform, and $\boldsymbol{I}_p = \boldsymbol{R}_{bm}\boldsymbol{R}_{ms}\boldsymbol{I}_{ps}(\boldsymbol{R}_{bm}\boldsymbol{R}_{ms})^{\mathrm{T}}$, $\boldsymbol{I}_{ps}$ denotes inertia tensor of top platform in the platform coordinate frame. Similarly, the generalized driving force of top platform can also be given by

$$\boldsymbol{F}_{pa} = \boldsymbol{J}_{\boldsymbol{ps}}^T m_p \boldsymbol{g} \tag{43}$$

where $\boldsymbol{g}$ is the gravity vector. It should be noted that driving forces are not included in the generalized driving force, however results are presented later in the dynamics equation.

Further, the generalized inertia force of cylinder rod can be given by, (44), as shown at th bottom of the next page, where m_{rc} denotes the mass of the cylinder rod; $\boldsymbol{I}_{rc}$ denotes the inertia tensor of cylinder rod with respect to the inertial reference frame. At the same time, the generalized driving force of cylinder rod can also be given by

$$\boldsymbol{F}_{rca} = \boldsymbol{J}_{\boldsymbol{rcs}}^T m_{rc} \boldsymbol{g} \tag{45}$$

Similarly the generalized inertia force of cylinder tube can be written as (46), shown at th bottom of the next page.

And the generalized driving force of cylinder tube is

$$\boldsymbol{F}_{tca} = \boldsymbol{J}_{\boldsymbol{tcs}}^T m_{tc} \boldsymbol{g} \tag{47}$$

$$\dot{\boldsymbol{J}}_p = \begin{bmatrix} -\boldsymbol{S}(\boldsymbol{\omega}_{sm} \times \boldsymbol{R}_{ms}\boldsymbol{\rho}^s)\boldsymbol{J}_{\omega sm} - \boldsymbol{S}(\boldsymbol{R}_{ms}\boldsymbol{\rho}^s)\dot{\boldsymbol{J}}_{\omega sm}, \dot{\boldsymbol{R}}_{bm}^T\boldsymbol{J}_{tm} - \boldsymbol{S}(\dot{\boldsymbol{t}}_s)\boldsymbol{R}_{bm}^T\boldsymbol{J}_{\omega m} - \boldsymbol{S}(\boldsymbol{t}_s)\dot{\boldsymbol{R}}_{bm}^T\boldsymbol{J}_{\omega m} - \\ \boldsymbol{S}(\boldsymbol{t}_s)\boldsymbol{R}_{bm}^T\dot{\boldsymbol{J}}_{\omega m} - \boldsymbol{S}(\boldsymbol{\omega}_{sm} \times \boldsymbol{R}_{ms}\boldsymbol{\rho}^s)\boldsymbol{R}_{bm}^T\boldsymbol{J}_{\omega m} - \boldsymbol{S}(\boldsymbol{R}_{ms}\boldsymbol{\rho}^s)\dot{\boldsymbol{R}}_{bm}^T\boldsymbol{J}_{\omega m} - \boldsymbol{S}(\boldsymbol{R}_{ms}\boldsymbol{\rho}^s)\boldsymbol{R}_{bm}^T\dot{\boldsymbol{J}}_{\omega m} \end{bmatrix} \tag{29}$$

$$\dot{\boldsymbol{J}}_{\omega m} = \begin{bmatrix} 0 & -\dot{\psi}_b\cos\psi_b & -\dot{\psi}_b\sin\psi_b\cos\theta_b - \dot{\theta}_b\cos\psi_b\sin\theta_b & 0 & 0 & 0 \\ 0 & -\dot{\psi}_b\sin\psi_b & \dot{\psi}_b\cos\psi_b\cos\theta_b - \dot{\theta}_b\sin\psi_b\sin\theta_b & 0 & 0 & 0 \\ 0 & 0 & -\dot{\theta}_b\cos\theta_b & 0 & 0 & 0 \end{bmatrix} \tag{30}$$

$$\dot{\boldsymbol{J}}_{\omega sm} = \begin{bmatrix} 0 & -\dot{\psi}_s\cos\psi_s & -\dot{\psi}_s\sin\psi_s\cos\theta_s - \dot{\theta}_s\cos\psi_s\sin\theta_s & 0 & 0 & 0 \\ 0 & -\dot{\psi}_s\sin\psi_s & \dot{\psi}_s\cos\psi_s\cos\theta_s - \dot{\theta}_s\sin\psi_s\sin\theta_s & 0 & 0 & 0 \\ 0 & 0 & -\dot{\theta}_s\cos\theta_s & 0 & 0 & 0 \end{bmatrix} \tag{31}$$

$$\dot{\boldsymbol{J}} = \dot{\boldsymbol{l}}_n^T\left(\boldsymbol{J}_{ts} - \boldsymbol{S}\left(\boldsymbol{R}_{ms}\boldsymbol{d}^s\right)\boldsymbol{J}_{\omega sm}\right) + \boldsymbol{l}_n^T\left(-\boldsymbol{S}\left(\boldsymbol{\omega}_{sm} \times \boldsymbol{R}_{ms}\boldsymbol{d}^s\right)\boldsymbol{J}_{\omega sm} - \boldsymbol{S}\left(\boldsymbol{R}_{ms}\boldsymbol{d}^s\right)\dot{\boldsymbol{J}}_{\omega sm}\right) \tag{34}$$

$$\dot{\boldsymbol{J}}_{arv} = \frac{\left(l\boldsymbol{S}\left(\dot{\boldsymbol{l}}_n\right) - \dot{l}\boldsymbol{S}\left(\boldsymbol{l}_n\right)\right)\left(\boldsymbol{J}_{ts} - \boldsymbol{S}\left(\boldsymbol{R}_{ms}\boldsymbol{d}^s\right)\boldsymbol{J}_{\omega sm}\right) - l\boldsymbol{S}\left(\boldsymbol{l}_n\right)\left(\boldsymbol{S}\left(\boldsymbol{\omega}_{sm} \times \boldsymbol{R}_{ms}\boldsymbol{d}^s\right)\boldsymbol{J}_{\omega sm} + \boldsymbol{S}\left(\boldsymbol{R}_{ms}\boldsymbol{d}^s\right)\dot{\boldsymbol{J}}_{\omega sm}\right)}{l^2} \tag{35}$$

$$\dot{\boldsymbol{J}}_{\omega arn} = \frac{\boldsymbol{l}_n^T\boldsymbol{h}_a\left(-\boldsymbol{i}_n\boldsymbol{h}_a^T\boldsymbol{J}_{arv} - \boldsymbol{l}_n\dot{\boldsymbol{h}}_a^T\boldsymbol{J}_{arv} - \boldsymbol{l}_n\boldsymbol{h}_a^T\dot{\boldsymbol{J}}_{arv}\right) - \left(\dot{\boldsymbol{l}}_n^T\boldsymbol{h}_a + \boldsymbol{l}_n^T\dot{\boldsymbol{h}}_a\right)\boldsymbol{l}_n\boldsymbol{h}_a^T\left(-\boldsymbol{J}_{arv}\right)}{\left(\boldsymbol{l}_n^T\boldsymbol{h}_a\right)^2} \tag{36}$$

$$\dot{\boldsymbol{J}}_{\omega a} = \left[\dot{\boldsymbol{J}}_{\omega ar}, \dot{\boldsymbol{R}}_{bm}^T\boldsymbol{J}_{\omega m} + \boldsymbol{R}_{bm}^T\dot{\boldsymbol{J}}_{\omega m}\right] \tag{37}$$

$$\dot{\boldsymbol{J}}_{rc} = \left(\left[0_{3\times 6}, \dot{\boldsymbol{J}}_{cb}\right] - d_{rc}\boldsymbol{S}\left(\dot{\boldsymbol{l}}_n\right)\boldsymbol{J}_{\omega a} - d_{rc}\boldsymbol{S}\left(\boldsymbol{l}_n\right)\dot{\boldsymbol{J}}_{\omega a}\right) \tag{38}$$

$$\dot{\boldsymbol{J}}_{tc} = \left(\dot{\boldsymbol{J}}_d + d_{tc}\boldsymbol{S}\left(\dot{\boldsymbol{l}}_n\right)\boldsymbol{J}_{\omega a} + d_{tc}\boldsymbol{S}\left(\boldsymbol{l}_n\right)\dot{\boldsymbol{J}}_{\omega a}\right) \tag{39}$$

Arranging the above equations, the mass matrix, the Coriolis/centripetal effects and gravity term can be obtained. Now, taking top platform as an example, the mass matrix and Coriolis /centripetal effects are obtained, respectively

$$\boldsymbol{M}_{ps} = \boldsymbol{J}_{ps}^{T} m_p \boldsymbol{J}_{ps} + \boldsymbol{J}_{\omega ss}^{T} \boldsymbol{I}_p \boldsymbol{J}_{\omega ss} \tag{48}$$

$$\boldsymbol{M}_{pb} = \boldsymbol{J}_{ps}^{T} m_p \boldsymbol{J}_{pb} + \boldsymbol{J}_{\omega ss}^{T} \boldsymbol{I}_p \boldsymbol{J}_{\omega sb} \tag{49}$$

$$\boldsymbol{C}_{ps} = \boldsymbol{J}_{ps}^{T} m_p \dot{\boldsymbol{J}}_{ps} + \boldsymbol{J}_{\omega ss}^{T} \boldsymbol{I}_p \dot{\boldsymbol{J}}_{\omega ss} + \boldsymbol{J}_{\omega ss}^{T} \boldsymbol{S}\left(\boldsymbol{\omega}_s\right) \boldsymbol{I}_p \boldsymbol{J}_{\omega ss} \tag{50}$$

$$\boldsymbol{C}_{pb} = \boldsymbol{J}_{ps}^{T} m_p \dot{\boldsymbol{J}}_{pb} + \boldsymbol{J}_{\omega ss}^{T} \boldsymbol{I}_p \dot{\boldsymbol{J}}_{\omega sb} + \boldsymbol{J}_{\omega ss}^{T} \boldsymbol{S}\left(\boldsymbol{\omega}_s\right) \boldsymbol{I}_p \boldsymbol{J}_{\omega sb} \tag{51}$$

Obviously, (49) and (51) indicate effects of ship motions on Stewart platform. It should be noted that the above analysis is aimed at top platform and one limb. When other limbs are considered, the complete dynamics model can be obtained

$$\boldsymbol{M}_s \ddot{\boldsymbol{q}}_s + \boldsymbol{C}_s \dot{\boldsymbol{q}}_s - \boldsymbol{G}_s + \boldsymbol{M}_m \ddot{\boldsymbol{q}}_b + \boldsymbol{C}_m \dot{\boldsymbol{q}}_b = \boldsymbol{J}^{T} \boldsymbol{f}_a \tag{52}$$

where $\boldsymbol{M}_s$, $\boldsymbol{C}_s$ and $\boldsymbol{G}_s$ denote the generalized mass matrix, centrifugal force & Coriolis force term and the gravity term, respectively. $\boldsymbol{f}_a$ denotes driving forces of six actuators.

Remark 1: The first two terms on the left side of (52) denote inertial forces induced by Stewart platform motions relative to the ship and the last two terms denote inertial forces induced by ship motions (disturbance forces). The influence of ship motions on the Stewart platform will be investigated in the latter section.

Remark 2: The Jacobian matrix $\boldsymbol{J}$ in (13) indicates that ship motions do not influence the singularity of Stewart platform. However, (52) shows that ship motions will influence the static force in practical application.

Property 1: For a real ship-mounted Stewart platform, ship motions can be conveniently measured by such motion sensors as Octans III equipped on the ship, then $\dot{\boldsymbol{q}}_b, \dot{\boldsymbol{q}}_b, \ddot{\boldsymbol{q}}_b$ can be obtained in real time and $\dot{\boldsymbol{q}}_b, \dot{\boldsymbol{q}}_b, \ddot{\boldsymbol{q}}_b \in L_\infty$.

III. MODEL ANALYSIS AND THE MODIFIED CONTROLLER

A. INFLUENCE FACTORS OF THE SHIP MOTIONS

Model in (52) indicates that the influence of ship motions on the Stewart platform contains the inertial forces. In addition, ship motions strongly affect the gravitational force term $\boldsymbol{G}_s$, since the pose of the Stewart platform changes with $\boldsymbol{R}_{bm}$ and $\boldsymbol{t}_m$. Now, influence factors [19-22] are utilized to quantitatively measure the effects of the ship motions on (52) in the compensation space.

1) Influence of the acceleration of ship motions In this end, we transformed (52) in the following form

$$\boldsymbol{M}_{ts} \ddot{\boldsymbol{q}}_s + \boldsymbol{C}_{ts} \dot{\boldsymbol{q}}_s - \boldsymbol{G}_t + \boldsymbol{M}_{tm} \ddot{\boldsymbol{q}}_b + \boldsymbol{C}_{tm} \dot{\boldsymbol{q}}_b = \boldsymbol{\tau}_a \tag{53}$$

with $\boldsymbol{M}_{ts} = \boldsymbol{J}^{-\mathrm{T}} \boldsymbol{M}_s$, $\boldsymbol{M}_{tm} = \boldsymbol{J}^{-\mathrm{T}} \boldsymbol{M}_m$, $\boldsymbol{C}_{ts} = \boldsymbol{J}^{-\mathrm{T}} \boldsymbol{C}_s$, $\boldsymbol{G}_{ts} = \boldsymbol{J}^{-\mathrm{T}} \boldsymbol{G}_s$. Then, influence factors for the acceleration of the ship is defined as

$$K_{as} = \max\left(\left|\boldsymbol{M}_{ts}\left(k, k\right)\right|\right) \tag{54}$$

$$K_{am} = \max\left(\left|\boldsymbol{M}_{tm}\left(k, k\right)\right|\right) \tag{55}$$

where, $k = 1,\ldots,6$. Obviously, the factors K_{as} and K_{am} are the maximum value of the magnitudes of the actuator forces due to the unit acceleration of the ship.

2) Influence of the velocity of ship motions In the same way, the influence factors for the velocity of the ship is defined as

$$K_{vs} = \max\left(\max\left(\left|\boldsymbol{C}_{ts} \boldsymbol{\lambda}_k'\right|\right)\right) \tag{56}$$

$$K_{vm} = \max\left(\max\left(\left|\boldsymbol{C}_{tm} \boldsymbol{\lambda}_k\right|\right)\right) \tag{57}$$

where, λ_k is the unit velocity vector of the ship and $\boldsymbol{\lambda}_k'$ can be calculated using (69)-(72). The physical meaning of K_{vs} and K_{vm} can be interpreted as the maximum value of the maximum magnitude of the actuator forces due to a unit velocity of the ship.

3) Influence on the gravity term Pose of the ship affects the gravity term, hence the influence factor is defined as

$$K_g = \max\left(\left|G_t\right|\right) \tag{58}$$

The above factors depend on the pose of the ship. Moreover, the subscript m in K_{am} and K_{vm} represents the effects of the ship motions on the inverse dynamics. When motion compensation is achieved, (53)-(58) can be calculated using (69)-(72). Hence, when the Stewart platform is at a pose with higher K_{as}, K_{vs}, K_{am}, K_{vm}, it requires larger actuator forces to maintain its pose.

B. MULTIPLE DEGREES OF FREEDOM VELOCITY FEEDFORWARD COMPENSATOR

Model in (52) fully describes the influence of ship motions on the Stewart platform, however, $\boldsymbol{q}_s$ is not the generalized position of top platform relative to inertial reference frame. Hence, we rewrite the model as the following form before implementing model analysis

$$\boldsymbol{M}_q \ddot{\boldsymbol{q}} + \boldsymbol{C}_q \boldsymbol{q} \dot{-} G_q + \boldsymbol{M}_b \ddot{\boldsymbol{q}}_b + \boldsymbol{C}_b \dot{\boldsymbol{q}}_b = \boldsymbol{J}^{T} \boldsymbol{f}_a = A \boldsymbol{J}^{T} \boldsymbol{p}_L \tag{59}$$

$$\boldsymbol{F}_p^I = -\boldsymbol{J}_{ps}^{T} m_p \left(\boldsymbol{J}_{ps} \ddot{\boldsymbol{q}}_s + \boldsymbol{J}_{pb} \ddot{\boldsymbol{q}}_b + \dot{\boldsymbol{J}}_{pb} \dot{\boldsymbol{q}}_b + \dot{\boldsymbol{J}}_{ps} \dot{\boldsymbol{q}}_s\right) - \boldsymbol{J}_{\omega ss}^{T} \left(\boldsymbol{I}_p \left(\boldsymbol{J}_{\omega sb} \ddot{\boldsymbol{q}}_b + \boldsymbol{J}_{\omega ss} \ddot{\boldsymbol{q}}_s + \dot{\boldsymbol{J}}_{\omega ss} \dot{\boldsymbol{q}}_s + \dot{\boldsymbol{J}}_{\omega sb} \dot{\boldsymbol{q}}_b\right) + \boldsymbol{S}\left(\boldsymbol{\omega}_s\right) \boldsymbol{I}_p \left(\boldsymbol{J}_{\omega ss} \dot{\boldsymbol{q}}_s + \boldsymbol{J}_{\omega sb} \dot{\boldsymbol{q}}_b\right)\right) \tag{42}$$

$$\boldsymbol{F}_{rc}^I = -\boldsymbol{J}_{\boldsymbol{rcs}}^{T} m_{rc} \left(\boldsymbol{J}_{rcb} \ddot{\boldsymbol{q}}_b + \boldsymbol{J}_{rcs} \ddot{\boldsymbol{q}}_s + \dot{\boldsymbol{J}}_{rcb} \dot{\boldsymbol{q}}_b + \dot{\boldsymbol{J}}_{rcs} \dot{\boldsymbol{q}}_s\right) - \boldsymbol{J}_{\omega as}^{T} \left(\boldsymbol{I}_{rc} \left(\boldsymbol{J}_{\omega ab} \ddot{\boldsymbol{q}}_b + \boldsymbol{J}_{\omega as} \ddot{\boldsymbol{q}}_s + \dot{\boldsymbol{J}}_{\omega ab} \dot{\boldsymbol{q}}_b + \dot{\boldsymbol{J}}_{\omega as} \dot{\boldsymbol{q}}_s\right) + \boldsymbol{S}\left(\boldsymbol{\omega}_a\right) \boldsymbol{I}_{rc} \left(\boldsymbol{J}_{\omega as} \dot{\boldsymbol{q}}_s + \boldsymbol{J}_{\omega ab} \dot{\boldsymbol{q}}_b\right)\right) \tag{44}$$

$$\boldsymbol{F}_{tc}^I = -\boldsymbol{J}_{\boldsymbol{tcs}}^{T} m_{tc} \left(\boldsymbol{J}_{tcb} \ddot{\boldsymbol{q}}_b + \boldsymbol{J}_{rcs} \ddot{\boldsymbol{q}}_s + \dot{\boldsymbol{J}}_{tcb} \dot{\boldsymbol{q}}_b + \dot{\boldsymbol{J}}_{tcs} \dot{\boldsymbol{q}}_s\right) - \boldsymbol{J}_{\omega as}^{T} \left(\boldsymbol{I}_{tc} \left(\quad \boldsymbol{J}_{\omega ab} \ddot{\boldsymbol{q}}_b + \boldsymbol{J}_{\omega as} \ddot{\boldsymbol{q}}_s + \dot{\boldsymbol{J}}_{\omega ab} \dot{\boldsymbol{q}}_b + \dot{\boldsymbol{J}}_{\omega as} \dot{\boldsymbol{q}}_s\right) + \boldsymbol{S}\left(\boldsymbol{\omega}_a\right) \boldsymbol{I}_{tc} \left(\boldsymbol{J}_{\omega as} \dot{\boldsymbol{q}}_s + \boldsymbol{J}_{\omega ab} \dot{\boldsymbol{q}}_b\right)\right) \tag{46}$$

with

$$\dot{\boldsymbol{q}} = \boldsymbol{H}\dot{\boldsymbol{q}}_b + \boldsymbol{T}\dot{\boldsymbol{q}}_s \tag{60}$$

where, $\boldsymbol{p}_L$ denotes the load pressure of the six hydraulic actuators. Since the above model is only utilized to carry out the theoretical analysis, we do not need to give specific formulates of variable symbols $\boldsymbol{M}_q, \boldsymbol{C}_q, \boldsymbol{G}_q, \boldsymbol{M}_b, \boldsymbol{C}_b, \boldsymbol{H}$ and $\boldsymbol{T}$. Compared with those fixed-base Stewart platforms, model in (59) presents stronger coupling. To facilitate the subsequent analysis, (59) is linearized at neutral position, and we utilize the same symbols with (59) to present the linearized model. Although the developed model cannot describe the entire behavior of the ship-mounted Stewart platform accurately, it is sufficient to generate certain control idea for the stabilization problem.

Since the frequencies of ship motion disturbances are mainly concentrated between 0.1 to 0.25 Hz, the top platform and base platform velocities remain relative low so that $\boldsymbol{C}_q\dot{\boldsymbol{q}}$ and $\boldsymbol{C}_b\dot{\boldsymbol{q}}_b$ can be ignored based on the subsequent analysis. Moreover, the main effect of the gravity term $\boldsymbol{G}_q$ is the static performance, i.e., steady-state error. Hence, in the following analysis, these terms are put aside.

In this study, the hydraulic actuators are chosen as for active control of the ship-mounted Stewart platform. The model of hydraulic actuator has been investigated widely, here, we utilize the model in [23]

$$\dot{\boldsymbol{p}}_L = \frac{4\beta_e}{V_t}(k_q\boldsymbol{u} - A\dot{\boldsymbol{l}} - k_{cs}\boldsymbol{p}_L) \tag{61}$$

where, β_e is the oil bulk modulus, k_q is the load pressure, $\boldsymbol{u}$ denotes input voltages of servo valves, k_{ce} is the leakage coefficient, V_t and A is total compressed volume and effective area of the hydraulic actuator, respectively.

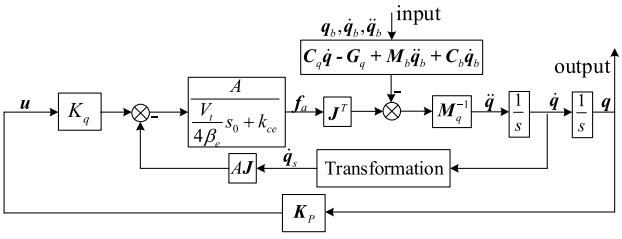

FIGURE 4. Block diagram of control system.

To present the frequency characteristics of the control system, a proportional control gain is utilized as position feedback and block diagram of control system is shown in Fig.4.

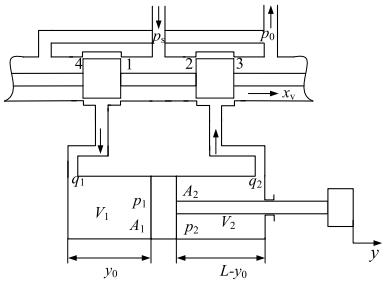

FIGURE 5. Schematic of the electrohydraulic actuator.

Furthermore, we take ship motions as the input signal and top platform motions as the output signal. Combining (13), (59), (60) and (61) and utilizing the Laplace-transform, the frequency characteristics from the input to the output can be obtained in (62), as shown at the bottom of the page, where, s_0 denotes the Laplace operator. If the proportional control gain $\boldsymbol{u}$=- $\boldsymbol{K}_P\boldsymbol{q}$ is chosen, then (62) can be rewritten as (63), shown at the bottom of the page.

It should be noted that as for hydraulic system, the term $k_{ce}+ s_0V_t/(4\beta_e)$ in (63) is approximately equal to 0, hence, it can be ignored. Equation (63) indicates that base motion velocity is the dominating factor contributing to platform motion. And, we cannot control base motions, hence we need to design a control law to make the amplitude of the frequency characteristics as small as possible in the desired frequency range. Now, we modified the control gain $\boldsymbol{u}$ in (62) as $\boldsymbol{u}_m$ =-$\boldsymbol{K}_P\boldsymbol{q}$-$A\boldsymbol{J}\boldsymbol{T}^{-1}\boldsymbol{H}s_0\boldsymbol{q}_b$/ k_q, equation (63) is reduced to, (64), as shown at the bottom of the page.

We can see that if the polynomial equation on the left side of (64) is stable, the amplitude of the frequency characteristics is approximately equal to 0. Obviously, the last term in $\boldsymbol{u}_m$ denotes a velocity feedforward compensator. Furthermore, we note that the term is the forced flow due to ship motions. In addition, we can also see that natural frequency is a significant index to guarantee stability of the polynomial equation and obtain better control performance. Namely, the higher it is, the larger the chosen $\boldsymbol{K}_P$ can be and the better control performance can obtain. Also, we can see that the integrator is a preferable choice to suppress the steady state error.

In the actual system, we should consider the nonlinear model in Stewart platform and hydraulic systems. Moreover, pose of top platform cannot be measured directly, we have to control the length of actuators to reach our target based on the measured ship motions and length of actuators. Herein, the

$$\left(\left(\frac{V_t}{4\beta_e}s_0 + k_{ce}\right)\boldsymbol{M}_q s_0^2 + A^2\boldsymbol{J}^T\boldsymbol{J}\boldsymbol{T}^{-1}s_0\right)\boldsymbol{q} = Ak_q\boldsymbol{J}^T\boldsymbol{u} + A^2\boldsymbol{J}^T\boldsymbol{J}\boldsymbol{T}^{-1}\boldsymbol{H}s_0\boldsymbol{q}_b - \left(\frac{V_t}{4\beta_e}s_0 + k_{ce}\right)\boldsymbol{M}_b s_0^2\boldsymbol{q}_b \tag{62}$$

$$\left(\left(\frac{V_t}{4\beta_e}s_0 + k_{ce}\right)\boldsymbol{M}_q s_0^2 + A^2\boldsymbol{J}^T\boldsymbol{J}\boldsymbol{T}^{-1}s_0 + Ak_q\boldsymbol{J}^T\boldsymbol{K}_P\right)\boldsymbol{q} = A^2\boldsymbol{J}^T\boldsymbol{J}\boldsymbol{T}^{-1}\boldsymbol{H}s_0\boldsymbol{q}_b - \left(\frac{V_t}{4\beta_e}s_0 + k_{ce}\right)\boldsymbol{M}_b s_0^2\boldsymbol{q}_b \tag{63}$$

$$\left(\left(\frac{V_t}{4\beta_e}s_0 + k_{ce}\right)\boldsymbol{M}_q s_0^2 + A^2\boldsymbol{J}^T\boldsymbol{J}\boldsymbol{T}^{-1}s_0 + Ak_q\boldsymbol{J}^T\boldsymbol{K}_P\right)\boldsymbol{q} = -\left(\frac{V_t}{4\beta_e}s_0 + k_{ce}\right)\boldsymbol{M}_b s_0^2\boldsymbol{q}_b \tag{64}$$

dynamics model of ship-mounted Stewart platform in the joint space is utilized and written as

$$\boldsymbol{M}_l\ddot{\boldsymbol{l}} + \boldsymbol{C}_l\dot{\boldsymbol{l}} - \boldsymbol{G}_l + \boldsymbol{M}_p\ddot{\boldsymbol{q}}_b + \boldsymbol{C}_p\dot{\boldsymbol{q}}_b = \boldsymbol{f}_a \tag{65}$$

with $\boldsymbol{M}_l = \boldsymbol{J}^{-T}\boldsymbol{M}_s\boldsymbol{J}^{-1}$, $\boldsymbol{C}_l = \boldsymbol{J}^{-T}\boldsymbol{C}_s\boldsymbol{J}^{-1} - \boldsymbol{J}^{-T}\boldsymbol{M}_s\boldsymbol{J}^{-1}\dot{\boldsymbol{J}}\boldsymbol{J}^{-1}$, $\boldsymbol{G}_l = \boldsymbol{J}^{-T}\boldsymbol{G}_s$, $\boldsymbol{M}_p = \boldsymbol{J}^{-T}\boldsymbol{M}_m$, $\boldsymbol{C}_p = \boldsymbol{J}^{-T}\boldsymbol{C}_m$. As for the drive system in each limb, the schematic diagram is shown in Fig. 5. To facilitate the theoretical analysis, assume that servo valve is the ideal, critical-center asymmetric valve. The ratio of area gradients of the spool ports is $w_2/w_1 = w_3/w_4 = m_0$. The sub-indexes 1 and 2 refer, respectively, to the rodless chamber and the rod chamber of a piston, $V_1 = V_{10} + A_1y_0$ and $V_2 = V_{20} - A_2y_0$ are volumes of the chambers with V_{10} and V_{20} corresponding to their initial values, and assume that $V_{10} \approx V_{20}$ holds. p_1 and p_2 are the chambers pressures, q_1 and q_2 are the flow rates through ports of the chambers, A_1 and A_2 are the ram areas of the two chambers, the area ratio of the asymmetric piston is $A_2 = A_1 = n_0$, $p_L = p_1 - n_0p_2$ is the load pressure, and y is the displacement of the piston, p_s denotes the supply pressure of a pump. Herein, the valve dynamics is neglected due to the low frequency range of wave spectrum and the actuator dynamics can be written as

$$\dot{\boldsymbol{p}}_L = \frac{\beta_e\left(1+n_0^2\right)}{V_{10}}\left(K_0\boldsymbol{f}\left(\tilde{\boldsymbol{p}}_L\right)\boldsymbol{u} - A_1\dot{\boldsymbol{l}} - C_{tc}\boldsymbol{p}_L\right) \tag{66}$$

where $K_0 = m_0Q_N/\left(V_N\sqrt{p_s/3.5/\left(n_0^3+m_0^2\right)}\right)$ is a constant, Q_N is the rated flow of servo valves, V_N is the rated voltage of servo valves, β_e is the oil bulk modulus, and C_{tc} is the equivalent leakage coefficient, $\boldsymbol{u}$ denotes input voltages of servo valves. Detailed derivations of the above equation are given in [24].

Based on the above analysis of velocity feedforward compensator, the forced flow due to ship motions can be calculated with

$$\begin{aligned}\boldsymbol{Q}_b &= A_1\left[\boldsymbol{L}_n^{\mathrm{T}} \quad (\boldsymbol{c}^{\boldsymbol{m}} \times \boldsymbol{L}_n)^{\mathrm{T}}\right]\begin{bmatrix}\boldsymbol{R}_{bm}^T & \boldsymbol{0}_{3\times3}\\ \boldsymbol{0}_{3\times3} & \boldsymbol{R}_{bm}^T\end{bmatrix}\begin{bmatrix}\boldsymbol{\omega}_m\\ \dot{\boldsymbol{t}}_m\end{bmatrix}\\ &= A_1\boldsymbol{J}_v\boldsymbol{v}_m\end{aligned} \tag{67}$$

where, $\boldsymbol{v}_m$ is the velocity of motion sensor expressed in the O_m. Furthermore, considering the nonlinearity of servo-valve flow, the multiple degrees of freedom velocity feedforward compensator is proposed as

$$\boldsymbol{u}_m = A_1\left(K_0\boldsymbol{f}\left(\tilde{\boldsymbol{p}}_L\right)\right)^{-1}\boldsymbol{J}_v\boldsymbol{v}_m \tag{68}$$

C. THE MODIFIED CONTROLLER

The previously mentioned, we have to control the length of actuators to keep top platform motionless in the inertial reference frame. Hence, we need to determine motion trajectory of top platform with respect to base platform given measured ship motions obtained from motion sensor. They can be calculated with the following equations

$$\theta_s = \arcsin\left(-\boldsymbol{R}_{bm}\left(1,3\right)\right) \tag{69}$$

$$\varphi_s = \arcsin\left(\boldsymbol{R}_{bm}\left(2,3\right)/\cos\theta_s\right) \tag{70}$$

$$\psi_s = \arcsin\left(\boldsymbol{R}_{bm}\left(1,2\right)/\cos\theta_s\right) \tag{71}$$

$$\boldsymbol{t}_s = \boldsymbol{R}_{bm}^T\left(\boldsymbol{t}_s^b - \boldsymbol{t}_m\right) \tag{72}$$

where $\boldsymbol{R}_{bm}(i;\,j)$ denotes the element in the i^{th} row and j^{th} column of the matrix $\boldsymbol{R}_{bm}$, $\boldsymbol{t}_s^b$ denotes position vector $\boldsymbol{t}_s$ in the inertial reference frame when the Stewart platform is at neutral position. With utilizing (5), desired length of the actuators can be calculated with

$$\boldsymbol{l}_d = \boldsymbol{t}_s + \boldsymbol{R}_{ms}\boldsymbol{d}^s - \boldsymbol{c}^m \tag{73}$$

Furthermore, the desired unit vector in the actuator direction $\boldsymbol{l}_{nd}$ can also be obtained and it can be utilized in controller design. As a result, the control objective of motion compensation is to make actual length of the actuators track desired length as closely as possible in spite of time-varying disturbances.

Considering the previous multiple degrees of freedom velocity feedforward compensator, the actuator dynamics (66) can be rewritten as

$$\dot{\boldsymbol{p}}_L = \beta_e\left(1+n_0^2\right)\left(\boldsymbol{u}_c - C_{tc}\boldsymbol{p}_L\right)/V_{10} \tag{74}$$

To stabilize (74), an inner loop controller is designed as

$$\boldsymbol{u}_c = \boldsymbol{K}_{pc}\tilde{\boldsymbol{p}}_L \tag{75}$$

where $\boldsymbol{K}_{pc}$ is a positive definite diagonal matrix of controller gain, $\tilde{\boldsymbol{p}}_L = \boldsymbol{p}_{Ld} - \boldsymbol{p}_L$ and $\boldsymbol{p}_{Ld}$ results from the outer controller. Furthermore, the outer loop controller is designed as

$$\begin{aligned}\boldsymbol{p}_{Ld} = \big(&-\boldsymbol{G}_l + \boldsymbol{M}_p\ddot{\boldsymbol{q}}_b\\ &+\boldsymbol{C}_p\dot{\boldsymbol{q}}_b + \boldsymbol{K}_p\left(\boldsymbol{l}_d - \boldsymbol{l}\right) + \boldsymbol{K}_I\int\left(\boldsymbol{l}_d - \boldsymbol{l}\right)dt\Big)/A_1\end{aligned} \tag{76}$$

where $\boldsymbol{K}_p$ and $\boldsymbol{K}_I$ are positive definite diagonal matrix of controller gain. And input voltages of servo valves can be summarized as

$$\boldsymbol{u} = \left(K_0\boldsymbol{f}\left(\tilde{\boldsymbol{p}}_L\right)\right)^{-1}\boldsymbol{K}_{pc}\tilde{\boldsymbol{p}}_L + A_1\left(K_0\boldsymbol{f}\left(\tilde{\boldsymbol{p}}_L\right)\right)^{-1}\boldsymbol{J}_v\boldsymbol{v}_m \tag{77}$$

Then, substituting (76) and (77) into (65) and (66), the conclusion that $(\boldsymbol{l}_d - \boldsymbol{l}) \in L_\infty$ can be obtained easily based on the error model.

In conclusion, the modified control method is illustrated in Fig.6.

Remark 3: Note that (77) includes the control input $\boldsymbol{u}$ on both sides of the equation since the controller input $\boldsymbol{u}$ is in the function $\boldsymbol{f}\left(\tilde{\boldsymbol{p}}_L\right)$, hence (77) cannot be obtained directly. Herein, the modified control law $\boldsymbol{u}$ is given out

$$\boldsymbol{u} = \left(K_0\boldsymbol{f}\left(\tilde{\boldsymbol{p}}_L, \boldsymbol{u}_b\right)\right)^{-1}\boldsymbol{u}_b \tag{78}$$

$$\boldsymbol{u}_b = \boldsymbol{K}_{pc}\tilde{\boldsymbol{p}}_L + A_1\boldsymbol{J}_v\boldsymbol{v}_m \tag{79}$$

Remark 4: Control method in [17], actuator velocity cannot be obtained directly and the influence of ship motions on the Stewart platform is not considered. Control method in [16], it is a kinematics control method based on the PID controller, it has a strict requirement on the frequency characteristics of

TABLE 1. Parameters of the ship-mounted Stewart platform.

Parameters	Value	Parameters	Value
r_c	1010 mm	r_d	1430 mm
d_c	200 mm	d_d	150 mm
h	1662.7 mm	$\boldsymbol{I}_{ps}$	diag(4095, 1908, 5687.5) kgm^2
$\boldsymbol{\rho}^s$	$(0, 0, -0.35)^T$ m		
C_{tc}	2×10^{-11} m^3/(s·Pa)	β_e	690 MPa
p_s	21 MPa	A_1	0.0031 m^2
A_2	0.0015 m^2	m_0	0.5
Q_N	250 L/min	V_N	10 V
m_p	21000 kg		

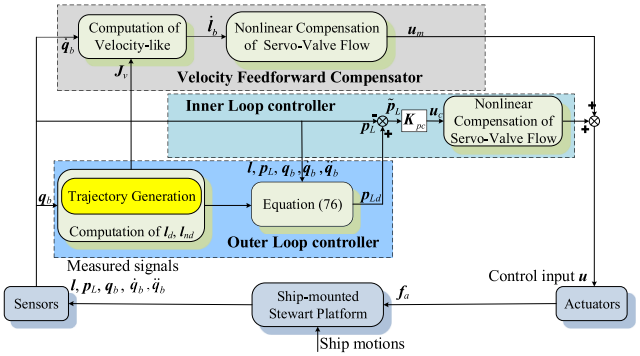

FIGURE 6. Block diagram of the modified control method.

the system, i.e. higher natural frequency is needed. Unlike the above control methods, the modified control method needs the velocity of motion sensor $\boldsymbol{v}_m$ which can be obtained from the motion sensor. Moreover, disturbance forces are fully considered and included in the outer loop controller.

Remark 5: There is a problem that calculating the Jacobian matrix $\boldsymbol{J}_v$ in multiple degrees of freedom velocity feedforward compensator needs kinematics forward solution. Herein, we utilize the above vector $\boldsymbol{l}_{nd}$ to avoid the process instead of $\boldsymbol{l}_n$. This is a controller simplification process.

Remark 6: To ensure the integrity of modeling theory, the multi-rigid-body dynamic model is established. However, as for the controller design, only top platform or load is needed to be included in the dynamics model since the most significant masses and inertias are top platform or load.

Remark 7: In the actuator model (see (66)), the term $-A_1\dot{\boldsymbol{l}}$ is omitted in (74). Although the actuator velocity contains the two components: one induced by motions of base platform or the ship $\dot{\boldsymbol{l}}_b$ and the other one induced by motions of top platform $\dot{\boldsymbol{l}}_p$, in practice, the main component is still generated by motions of base platform for a good ship-mounted Stewart platform. In other words, the velocity term in (66) is compensated for with minor error.

Remark 8: Based on **Remark 7**, a preferable choice is to utilize $\dot{\boldsymbol{l}}_b$ to replace the actuator velocity. Then the disturbance forces compensation can be achieved using the replacement, similar control performance can be obtained. This is also a controller simplification process.

IV. SIMULATION RESULTS

A. DYNAMIC PERFORMANCE SIMULATION

To present the influence of ship motions on the Stewart platform, we investigate the distribution of the influence factors K_{as}, K_{vs}, K_{am}, K_{vm} and K_g, which are nonlinear functions of $\boldsymbol{q}_b$. In practical applications, since horizontal motions of a ship are usually controlled by a dynamic positioning system, the main components of the ship motions are roll, pitch and heave. Hence, the factors about θ_b, φ_b and z_b are calculated when motion compensation is achieved, i.e. top platform keep motionless. The main parameters of the ship-mounted Stewart platform are listed in Table 1.

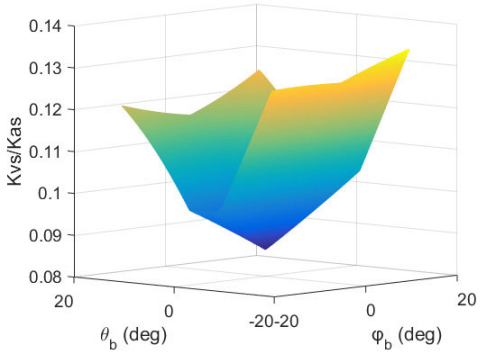

FIGURE 7. Distribution of K_{vs}/K_{as}.

Considering different dimensions of translational and rotational motion, for the ship, a translation with a unit linear velocity or acceleration is input while 0.4 of a unit velocity or acceleration is input for the rotational motion since a unit rotation velocity is too large for the wave induced ship motions. Now, we investigate the influence of velocity and acceleration term on the inverse dynamics and the result is shown in Fig.7 when the pose of the ship are $x_b = y_b = z_b = 0$ and $\psi_b = 0$.

As shown in Fig.7, the distribution shows that the maximum value of K_{vs}/K_{as} is 0.135 and the minimum value is 0.08 when the Stewart platform is at neutral position. This indicates that the acceleration term $\boldsymbol{M}_s\ddot{\boldsymbol{q}}_s$ has a more significant impact on actuator force compared with the velocity

term $\boldsymbol{C}_s\dot{\boldsymbol{q}}_s$. In other words, in the subsequent model analysis, the term $\boldsymbol{C}_s\dot{\boldsymbol{q}}_s$ can be ignored. The same conclusion can be obtained for the term $\boldsymbol{C}_m\dot{\boldsymbol{q}}_b$ although the distribution of K_{vb}/K_{ab} is not given out.

Furthermore, we investigate the influence of ship motions on the gravitational term. The result is shown in Fig.8 when the pose of the ship are $x_b = y_b = 0$ and $\psi_b = 0$.

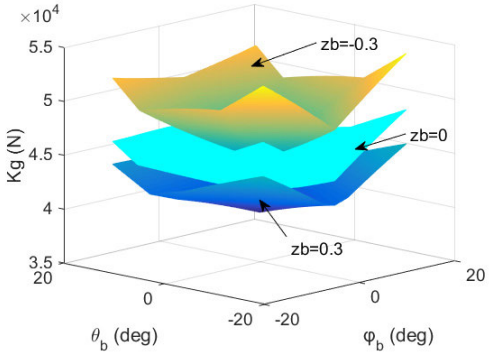

FIGURE 8. Distribution of K_g.

As shown in Fig.8, the distribution of K_g shows as the base platform moves closer to the top platform (z_b becomes smaller), the Stewart platform requires larger actuator forces to maintain the pose and the added value is about 2500N. It can be seen that the Euler angles θ_b and φ_b also have effect on the inverse dynamics and the difference between the maximum and the minimum is about 7000N. Hence, compared to the Euler angles, the displacement z_b has relatively minor influence on the gravitational force term.

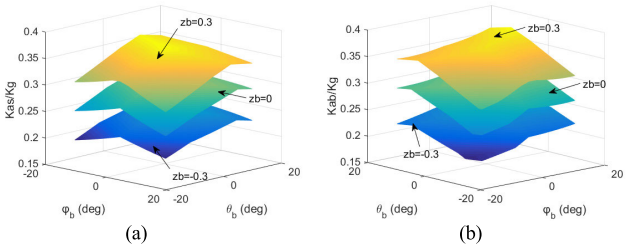

FIGURE 9. Influence of acceleration term: (a) distribution of K_{as}/K_g and (b) distribution of K_{am}/K_g.

Finally, we investigate the influence of acceleration terms on the inverse dynamics and the results are shown in Fig.9 when the pose of the ship are $x_b = y_b = 0$ and $\psi_b = 0$.

As shown in Fig.9, the gravitational force term has a significant impact on the actuator forces compared with the acceleration term $\boldsymbol{M}_s\ddot{\boldsymbol{q}}_s$ and $\boldsymbol{M}_m\ddot{\boldsymbol{q}}_b$, however, the acceleration terms cannot be ignored. And the acceleration term $\boldsymbol{M}_s\ddot{\boldsymbol{q}}_s$ has a similar effect on the dynamics model with $\boldsymbol{M}_m\ddot{\boldsymbol{q}}_b$. Specially, as the base platform moves closer to the top platform (z_b becomes smaller), the acceleration term has smaller effect on actuator forces.

B. CONTROL SYSTEM SIMULATION

In this subsection, simulations are provided to further verify the effectiveness of the modified control method. A dynamics simulator is built in the MATLAB/Simulink environment in which the motion sensor (e.g. Octans III) gives motions of base platform to the controller. The actuator stroke range is assigned to be from -0.41m to +0.44m and the other parameters of the ship-mounted Stewart platform are still listed in Table 1.

The initial pose of top platform in the attached reference frame O_m are set as

$$\boldsymbol{q}_s = [0, 0, 0, 0, 0, -h]^T \tag{80}$$

$$\boldsymbol{q}_m = [0, 0, 0, 0, 0, 0]^T \tag{81}$$

To my knowledge, there are not many results about stabilization problem of ship-mounted Stewart platform, Hence, in this study, three control methods are compared: 1) Control method in [16] i.e. PID controller with pressure feedback A PID controller with pressure feedback is tested for comparison. The control law $\boldsymbol{u}_{pi}$ is

$$\boldsymbol{u}_{pi} = \boldsymbol{K}_p\left(\boldsymbol{l}_d - \boldsymbol{l}\right) + \boldsymbol{K}_I\int\left(\boldsymbol{l}_d - \boldsymbol{l}\right)dt - \boldsymbol{K}_{dp}\boldsymbol{p}_L \tag{82}$$

After sufficient tuning, a group of controller parameters are selected as $\boldsymbol{K}_p = \text{diag}\ \{100;\ 100;\ 100;\ 100;\ 100;\ 100\}$ $\boldsymbol{K}_I = \text{diag}\ \{70;\ 70;\ 70;\ 70;\ 70;\ 70\}$, $K_{dp} = 1 \times 10^{-7}$.

2) Control method in [17] i.e. Inverse dynamics control

An inverse dynamics controller is tested for comparison. The outer loop control law $\boldsymbol{u}_{olc}$ is

$$\boldsymbol{u}_{olc} = \boldsymbol{K}_p\left(\boldsymbol{l}_d - \boldsymbol{l}\right) - \boldsymbol{J}^T\boldsymbol{G}_{s0}/A_1 \tag{83}$$

where, $\boldsymbol{G}_{s0}$ denotes the gravity vector at neutral position. The inner loop control law $\boldsymbol{u}_{ilc}$ is

$$\boldsymbol{u} = \boldsymbol{K}_{pc}\tilde{\boldsymbol{p}}_L + A_1\left(K_0\boldsymbol{f}\left(\bar{\boldsymbol{p}}_L\right)\right)^{-1}\dot{\boldsymbol{l}} \tag{84}$$

A group of controller parameters are selected as

$\boldsymbol{K}_p = \text{diag}\ \{5 \times 10^6; 5 \times 10^6; 5 \times 10^6; 5 \times 10^6; 5 \times 10^6; 5 \times 10^6\}$,

$\boldsymbol{K}_{pc} = \text{diag}\ \{4 \times 10^{-7}; 4 \times 10^{-7}; 4 \times 10^{-7}; 4 \times 10^{-7}; 4 \times 10^{-7}; 4 \times 10^{-7}\}$.

3) The modified controller

The control parameters are set as

$\boldsymbol{K}_p = \text{diag}\ \{4.8 \times 10^6; 4.8 \times 10^6; 4.8 \times 10^6; 4.8 \times 10^6; 4.8 \times 10^6; 4.8 \times 10^6\}$,

$\boldsymbol{K}_I = \text{diag}\ \{3 \times 10^6; 3 \times 10^6; 3 \times 10^6; 3 \times 10^6; 3 \times 10^6; 3 \times 10^6\}$,

$\boldsymbol{K}_{pc} = \text{diag}\ \{4 \times 10^{-11}; 4 \times 10^{-11}; 4 \times 10^{-11}; 4 \times 10^{-11}; 4 \times 10^{-11}; 4 \times 10^{-11}\}$.

On the consideration that the control object is to keep the top platform motionless relative to the inertial reference frame all the time, thus the pose deviation in the inertial reference frame is used as motion compensation error to evaluate control system performance, and the error is also motion response of top platform to ship motion-induced perturbations. For fair comparison, all control parameters are fixed for different motion disturbance cases.

Since the ship-mounted Stewart platform can compensate for the full degrees of freedom motions of a ship, single degree of freedom motion simulations and multi-degree of freedom motion simulations are carried out to verify control performance of the proposed controller. Firstly, single degree of freedom motions obtained from the motion sensor are given for the heave disturbance motion and roll motion disturbance, respectively. Since the frequencies of ship motion disturbances are mainly concentrated between 0.1 to 0.25 Hz, motions (heave and roll) are assumed to be equal to sin(·)-waves

$$z_b = 0.4 \sin(2\pi \omega_{dis} t) \tag{85}$$

$$\varphi_b = 13 \sin(2\pi \omega_{dis} t) \tag{86}$$

propagating with a variable frequency, starting with $\omega_{dis} = 0$ and ending with $\omega_{dis} = 0.3$ Hz as shown in Fig.10.

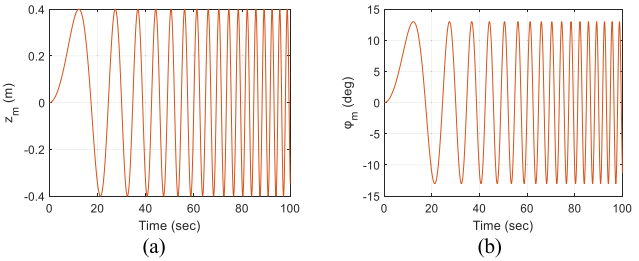

FIGURE 10. Single degree of freedom motion simulations: (a) ship heave motion disturbance and (b) ship roll motion disturbance.

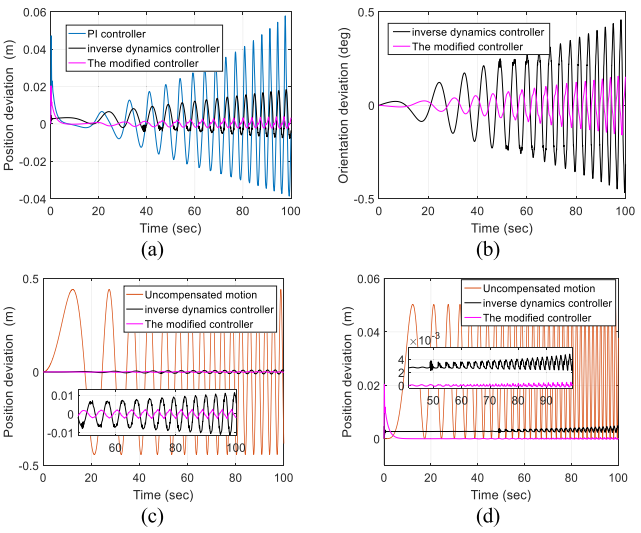

FIGURE 11. Position and orientation deviation of top platform: (a) Position deviation in the z-direction with ship heave motion disturbance. (b) Orientation deviation in the Rx direction with ship roll motion disturbance, (c) Position deviation in the y-direction with ship roll motion disturbance and (d) Position deviation in the z-direction with ship roll motion disturbance.

For the single degree of freedom motion simulations, Fig.11(a) shows the z-direction response of top platform to the heave motion disturbance and Fig.11(b)-(d) present the rotation, y-direction and z-direction response of top platform to the roll motion disturbance using different controllers, i.e., PI controller, the inverse dynamics controller and the modified controller. When ship roll motion disturbance is input, existing control strategy i.e. PI controller is unstable. In addition, parasitic motions in y and z-direction are presented with red lines in Fig.11(c) and (d). Maximum values are 0.44m and 0.05m, respectively. Comparing purple with black lines in Fig.11, we can see that the modified controller has better performance and its maximum motion compensation error is 4mm, 0.16deg, 2.5mm, 0 in the subfigures, while maximum compensation error of inverse dynamics controller is 18mm, 0.46deg, 11.5mm, 4.8mm. Then, we mainly compare control performance of inverse dynamics controller and the modified controller.

Besides the above single degree of freedom simulations, 3 degrees of freedom simulations (heave, roll and pitch) are carried out. Herein, we select sinusoidal signals with a fixed amplitude and frequency in this case. The ship motion disturbances are chosen as $z_b = 0.2\sin(2\pi t/8)$, $\varphi_b = 8\sin(2\pi t/10)$ and $\theta_b = 5\sin(2\pi t/5)$.

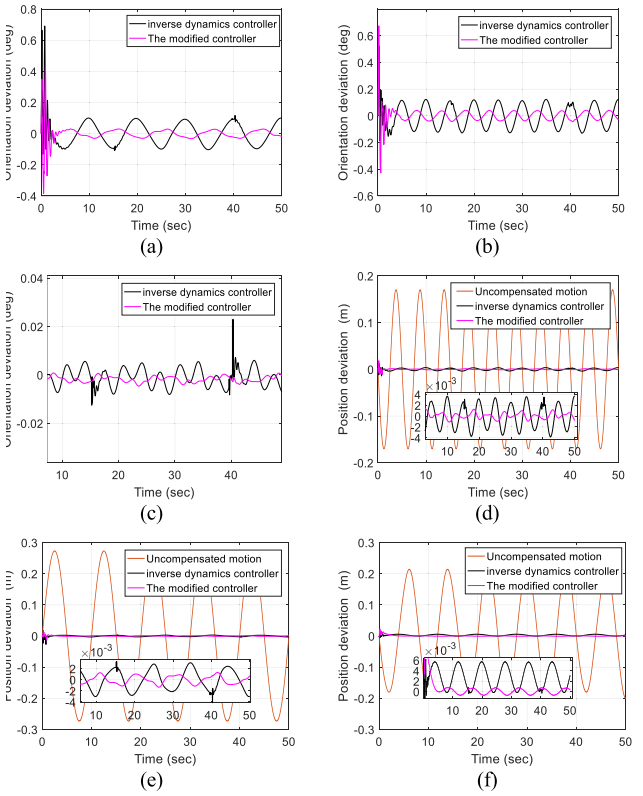

FIGURE 12. Results of 3 degrees of freedom simulation: (a) Orientation deviation in the Rx-direction, (b) Orientation deviation in the Ry-direction, (c) Orientation deviation in the Rz-direction and (d) Position deviation in the x-direction, (e) Position deviation in the y-direction, (f) Position deviation in the z-direction.

Fig.12 shows 6 degrees of freedom motion responses of top platform to 3 degrees of freedom motion disturbances. Red lines in Fig.12 shows that maximum values of parasitic motions in the x, y and z-direction are 170mm, 273mm and 215mm. Compared with black and purple lines in the

subplots, maximum values of motion responses in 6 degrees of freedom are 0.1deg, 0.13deg, 0.02deg, 3.5mm, 3mm and 6mm using the inverse dynamics controller and the maximum values are 0.03deg, 0.04deg, 0, 1.1mm, 1.3mm and 0.8mm using the modified controller. Obviously, the modified controller has better control performance.

In addition to the above simulations, the ship-mounted Stewart platform is utilized in the field of ocean engineering. Hence, random signals generated by wave spectrum are utilized to test convergence properties of the proposed controller. Simulated signals of ship motion-induced perturbations (heave and roll motion disturbances) are generated by using stochastic wave motion theory based on the JONSWAP spectrum with the help of the Marine System Simulator (MSS) toolbox for MATLAB ([25], [26]). The two parameters of the wave spectrum are defined by the peak period T_p and the significant wave height H_s. Considering the limited stroke lengths of actuators, the two parameters are set as $T_p = 5s$ and $H_s = 0.6m$. And the random signals for heave and roll motion disturbances are shown in Fig.13.

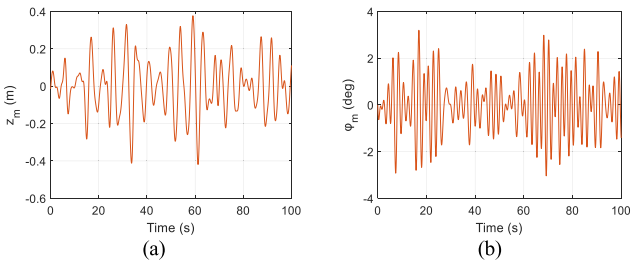

FIGURE 13. Random signal inputs: (a) ship heave motion disturbance and (b) ship roll motion disturbance.

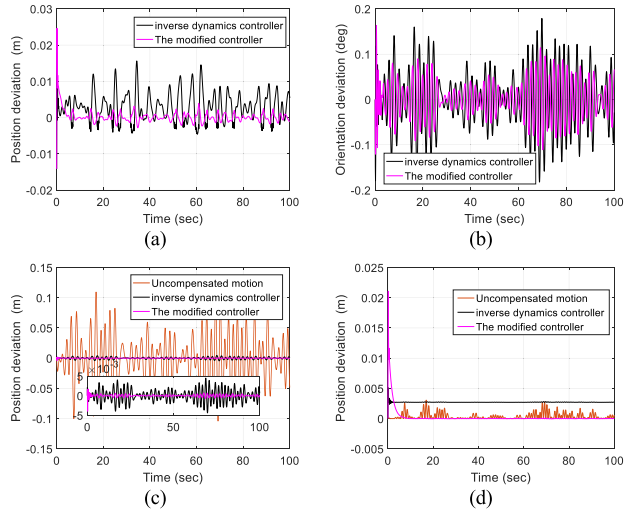

FIGURE 14. Simulation results for the random signals: (a) Position deviation in the z-direction with ship heave motion disturbance. (b) Orientation deviation in the Rx-direction with ship roll motion disturbance, (c) Position deviation in the y-direction with ship roll motion disturbance and (d) Position deviation in the z-direction with ship roll motion disturbance.

For the above random signal inputs, Fig.14(a) shows the z-direction response for the heave motion disturbance and Fig.14(b)-(d) present the rotation, y-direction and z-direction response for the roll motion disturbance. By contrast, without retuning the control parameters, the same conclusion is reached and the modified controller (purple lines) maintains excellent control performance which is consistent with the previous conclusions. And the above simulation results indicate satisfactory performance of the modified control method.

V. CONCLUSION

In this paper, a modified control method has been proposed for the ship-mounted Stewart platform for wave compensation. The control method consists of velocity feedforward loop and motion control loop. Specifically, the dynamics model considering the influence of ship motions on the Stewart platform is established and the influence of ship motions on the Stewart platform is analyzed. Then, through the model analysis, a multiple degrees of freedom velocity feedforward compensator is proposed. Furthermore, a modified motion controller including inner loop feedback controller and the outer loop position controller is developed. Model analysis results indicate that the gravitational force term has a significant impact on the actuator forces compared with inertial forces and that inertial forces coming from velocity terms can be ignored. Finally, simulations are included to illustrate the effectiveness of the modified control method by contrast.

REFERENCES

[1] F. A. Leban, J. Diaz-Gonzalez, G. G. Parker, and W. Zhao, "Inverse kinematic control of a dual crane system experiencing base motion," *IEEE Trans. Control Syst. Technol.*, vol. 23, no. 1, pp. 331–339, Jan. 2015, doi: 10.1109/TCST.2014.2314020.

[2] S. S. Tordal and G. Hovland, "Inverse kinematic control of an industrial robot used in vessel-to-vessel motion compensation," in *Proc. 25th Medit. Conf. Control Autom. (MED)*, Valletta, Malta, Jul. 2017, pp. 1392–1397.

[3] Y. Fang, P. Wang, N. Sun, and Y. Zhang, "Dynamics analysis and nonlinear control of an offshore boom crane," *IEEE Trans. Ind. Electron.*, vol. 61, no. 1, pp. 414–427, Jan. 2014, doi: 10.1109/TIE.2013.2251731.

[4] N. Sun, Y. Fang, H. Chen, Y. Fu, and B. Lu, "Nonlinear stabilizing control for ship-mounted cranes with ship roll and heave movements: Design, analysis, and experiments," *IEEE Trans. Syst., Man, Cybern. Syst.*, vol. 48, no. 10, pp. 1781–1793, Oct. 2018.

[5] B. Lu, Y. Fang, N. Sun, and X. Wang, "Antiswing control of offshore boom cranes with ship roll disturbances," *IEEE Trans. Control Syst. Technol.*, vol. 26, no. 2, pp. 740–747, Mar. 2018, doi: 10.1109/TCST.2017.2679060.

[6] T. I. Fossen, *Handbook of Marine Craft Hydrodynamics and Motion Control*. Chichester, U.K.: Wiley, 2011.

[7] T. I. Fossen, *Guidance and Control of Ocean Vehicles*. New York, NY, USA: Wiley, 1994.

[8] S. Küchler, T. Mahl, J. Neupert, K. Schneider, and O. Sawodny, "Active control for an offshore crane using prediction of the vessel's motion," *IEEE/ASME Trans. Mechatronics*, vol. 16, no. 2, pp. 297–309, Apr. 2011, doi: 10.1109/TMECH.2010.2041933.

[9] B. He, Y. Fang, N. Sun, and H. Chen, "Adaptive nonlinear crane control with load hoisting/lowering and unknown parameters: Design and experiments," *IEEE/ASME Trans. Mechatronics*, vol. 20, no. 5, pp. 297–309, Oct. 2015, doi: 10.1109/TMECH.2014.2364308.

[10] N. Sun, Y. Fang, H. Chen, Y. Wu, and B. Lu, "Nonlinear antiswing control of offshore cranes with unknown parameters and persistent ship-induced perturbations: Theoretical design and hardware experiments," *IEEE Trans. Ind. Electron.*, vol. 65, no. 3, pp. 2629–2641, Mar. 2018, doi: 10.1109/TIE.2017.2767523.

[11] D. Salzmann, "Development of the access system for offshore wind turbines," Ph.D. dissertation, Dept. Hydr. Eng., Delft Univ. Technol., Delft, The Netherlands, 2010.

[12] A. L. Madsen and S. G. Kristensen, "Design of Stewart platform for wave compensation," M.S. thesis, Dept. Mech. Prod., Aalborg Univ., Aalborg, Denmark, 2012.
[13] Z. Chang, Z. Chen, Z. Zheng, Y. Yang, X. Zhou, and J. He, "Compensation space analysis of motion compensation device for offshore floating platform," *Periodical Ocean Univ. China*, vol. 49, no. 12, pp. 116–121, Dec. 2019, doi: 10.16441/j.cnki.hdxb.20170352.
[14] A. Wang, Y. Wei, H. Han, L. Guan, X. Zhang, and X. Xu, "Ocean wave active compensation analysis of inverse kinematics for hybrid boarding system based on fuzzy algorithm," in *Proc. OCEANS-MTS/IEEE Kobe Techno-Oceans (OTO)*, Harbin, China, May 2018, pp. 1–6.
[15] T.-S. Zhao, C. Wang, X. Liu, H. Bian, and Y.-Z. Zhao, "Stiffness and singularity analysis of foldable parallel mechanism for ship-based stabilized platform," *Robotica*, vol. 34, no. 4, pp. 913–924, Apr. 2016, doi: 10.1017/S0263574714001969.
[16] A. Campos, J. Quintero, R. Saltaren, M. Ferre, and R. Aracil, "An active helideck testbed for floating structures based on a Stewart-Gough platform," in *Proc. IEEE/RSJ Int. Conf. Intell. Robots Syst.*, Nice, France, Sep. 2008, pp. 22–26.
[17] K. Lie, "Inverse dynamics control for the Ampelmann system," M.S. thesis, Dept. Syst. Control, Delft Univ. Technol., Delft, The Netherlands, 2017.
[18] M. Vakil, H. Pendar, and H. Zohoor, "Comments to the: 'Closed-form dynamic equations of the general Stewart platform through the Newton-Euler approach' and 'a Newton-Euler formulation for the inverse dynamics of the Stewart platform manipulator,'" *Mechanism Mach. Theory*, vol. 102, no. 10, pp. 229–231, Aug. 2016, doi: 10.1016/j.mechmachtheory.2016.04.003.
[19] Y. Li, F. Xi, A. D. Finistauri, and K. Behdinan, "Dynamic modeling and analysis of a circular track-guided tripod," *J. Comput. Nonlinear Dyn.*, vol. 5, no. 1, pp. 125–133, Apr. 2010, doi: 10.1115/1.4000313.
[20] Y. Zhao and F. Gao, "Dynamic formulation and performance evaluation of the redundant parallel manipulator," *Robot. Comput.-Integr. Manuf.*, vol. 25, nos. 4–5, pp. 770–781, Aug. 2009, doi: 10.1016/j.rcim.2008.10.001.
[21] Y. Li, J. Wang, X.-J. Liu, and L.-P. Wang, "Dynamic performance comparison and counterweight optimization of two 3-DOF parallel manipulators for a new hybrid machine tool," *Mechanism Mach. Theory*, vol. 45, no. 11, pp. 1668–1680, Nov. 2010, doi: 10.1016/j.mechmachtheory.2010.06.009.
[22] Y. Zhao and F. Gao, "Dynamic performance comparison of the 8PSS redundant parallel manipulator and its non-redundant counterpart—The 6PSS parallel manipulator," *Mechanism Mach. Theory*, vol. 44, no. 5, pp. 991–1008, May 2009, doi: 10.1016/j.mechmachtheory.2008.05.015.
[23] H. E. Merritt, *Hydraulic Control Systems*. New York, NY, USA: Wiley, 1967.
[24] H. Guo, Y. Liu, G. Liu, and H. Li, "Cascade control of a hydraulically driven 6-DOF parallel robot manipulator based on a sliding mode," *Control Eng. Pract.*, vol. 16, no. 9, pp. 1055–1068, Sep. 2008, doi: 10.1016/j.conengprac.2007.11.005.
[25] T. I. Fossen, *Marine Control Systems*, Trondheim, Norway: Marine Cybernetics AS, 2002.
[26] W. J. Pierson and L. Moskowitz, "A proposed spectral form for fully developed wind seas based on the similarity theory of S. A. Kitaigorodskii," *J. Geophys. Res.*, vol. 69, no. 24, pp. 5181–5190, Dec. 1964, doi: 10.1029/JZ069i024p05181.

YUNFEI CAI received the M.S. degree in mechatronic engineering from the Harbin Institute of Technology, Harbin, China, in 2017, where he is currently pursuing the Ph.D. degree in mechanical engineering.

His research interests include stabilizing control of ship-mounted Stewart platforms and dynamics and control of parallel manipulators.

SHUTAO ZHENG received the B.E., M.E., and Ph.D. degrees in mechanical engineering from the Harbin Institute of Technology, Harbin, China, in 2001, 2003, and 2009, respectively.

He is currently an Associate Professor with the Institute of Electro-Hydraulic Servo Simulation and Test System, Harbin Institute of Technology. His current research interests include flight simulation, dynamics and control of parallel manipulators, and control of redundant shaking table.

WEITIAN LIU received the M.S. degree in mechatronic engineering from the Harbin Institute of Technology, Harbin, China, in 2017.

He joined the Aecc Aero Engine Control System Institute, Aero Engine Corporation of China, Wuxi, China, in 2017. His current research interest includes aero-engine load effect simulation.

ZHIYONG QU received the B.E. and M.E. degrees in mechanical manufacture and automation, and the Ph.D. degree in navigation, guidance and control from the Harbin Institute of Technology, Harbin, China, in 2000, 2002, and 2008, respectively.

He is currently an Associate Professor with the Institute of Electro-Hydraulic Servo Simulation and Test System, Harbin Institute of Technology. His current research interests include dynamics and control of parallel manipulators and adaptive control of redundant shaking table.

JUNWEI HAN received the B.E., M.E., and Ph.D. degrees in fluid transmission and control from the Harbin Institute of Technology, Harbin, China, in 1986, 1989, and 1992, respectively.

From 1992 to 1994, he was a Postdoctoral Fellow with the Institute of Engineering Mechanics, China Earthquake Administration, Harbin. From 1994 to 1997, he was a Postdoctoral Fellow with the School of Mechanical and Electrical Engineering, Harbin Institute of Technology. He is currently a Professor with the Institute of Electro-Hydraulic Servo Simulation and Test System, Harbin Institute of Technology. His research interests include dynamics and control of parallel manipulators, control of redundant shaking table, theory and application of electro-hydraulic servo systems.